Modulation of Concentration Fluctuations in Phase-Separated Lipid Membranes by Polypeptide Insertion

S. Fahsel,* E.-M. Pospiech,* M. Zein,* T. L. Hazlet,† E. Gratton,† and Roland Winter*
University of Dortmund, Department of Chemistry, Physical Chemistry I, D-44221 Dortmund, Germany; and †Laboratory for Fluorescence Dynamics, University of Illinois, Urbana, Illinois 61801 USA

ABSTRACT The lateral membrane organization and phase behavior of the binary lipid mixture DMPC (1,2-dimyristoyl-*sn*-glycero-3-phosphatidylcholine) - DSPC (1,2-distearoyl-*sn*-glycero-3-phosphatidylcholine) without and with incorporated gramicidin D (GD) as a model biomembrane polypeptide was studied by small-angle neutron scattering, Fourier-transform infrared spectroscopy, and by two-photon excitation fluorescence microscopy on giant unilamellar vesicles. The small-angle neutron scattering method allows the detection of concentration fluctuations in the range from 1 to 200 nm. Fluorescence microscopy was used for direct visualization of the lateral lipid organization and domain shapes on a micrometer length scale including information of the lipid phase state. In the fluid-gel coexistence region of the pure binary lipid system, large-scale concentration fluctuations appear. Infrared spectral parameters were used to determine the peptide conformation adopted in the different lipid phases. The data show that the structure of the temperature-dependent lipid phases is significantly altered by the insertion of 2 to 5 mol% GD. At temperatures corresponding to the gel-fluid phase coexistence region the concentration fluctuations drastically decrease, and we observe domains in the giant unilamellar vesicles, which mainly disappear by the incorporation of 2 to 5 mol% GD. Further, the lipid matrix has the ability to modulate the conformation of the inserted polypeptide. The balance between double-helical and helical dimer structures of GD depends on the phospholipid chain length and phase state. A large hydrophobic mismatch, such as in gel phase one-component DSPC bilayers, leads to an increase in population of double-helical structures. Using an effective molecular sorting mechanism, a large hydrophobic mismatch can be avoided in the DMPC-DSPC lipid mixture, which leads to significant changes in the heterogeneous lipid structure and in polypeptide conformation.

INTRODUCTION

The lipid lateral organization poses one of the major current problems in the biophysics of biomembranes (Lipowsky and Sackmann, 1995; Jørgensen et al., 1993, 2000; Jørgensen and Mouritsen, 1995, Winter et al., 1999). A particular question is related to the existence of lipid domains on the nanometer (1–100 nm) and micrometer scale and the relationship between lipid-domain formation and the conformation and functional properties of membrane-associated proteins. Formation of (dynamic) lipid domains is a mere consequence of the many-particle nature of biological membranes. In the case of equilibrium, phase separation leads to the formation of macroscopically large domains (phases), whereas out of equilibrium, the phase separation process may produce small-scale domains, and compositional fluctuations may be observed. The domains may have a local composition that is different from the global composition in the phase under consideration, and it has been conjectured that the multicomponent character of biomembranes may lead to strong membrane heterogeneity and phase segregation originating from compositional fluctuations. Some experimental and theoretical evidence is available now that supports the existence of this type of heterogeneity already in two-component lipid bilayer systems (Jørgensen et al., 1993, 2000; Jørgensen and Mouritsen, 1995; Gliss et al., 1998; Winter et al., 1999; Sugár et al., 1999; Nielsen et al., 2000).

When an integral membrane protein is incorporated into lipid membrane systems, which are subject to this kind of lipid domain formation, the domain formation may be modulated by the presence of the protein in a way that reflects the lipid-protein interactions. On the other hand, the domain structure will influence the tension of the protein, which in some cases may introduce conformational changes in the protein and, therefore, couple indirectly to the protein function (Sankaram et al., 1994; Dumas et al., 1997; Schram and Thompson, 1997; Gil et al., 1998; Curran et al., 1999; Estrela-Lopis et al., 2000; Cornelius, 2001; Hinderliter et al., 2001; Davies et al., 2001; May and Ben-Shaul, 2000).

Turning to the molecular mechanisms involved in lipid-protein interactions, hydrophobic matching of lipid-bilayer thickness and hydrophobic thickness of integral proteins has been proposed as an important parameter. In the case of a binary lipid system consisting of lipid species with different hydrophobic chain lengths, the hydrophobic matching principle has been proposed to act as a mechanism for lipid sorting at the lipid-protein interface because the protein will, on a statistical basis, prefer to be associated with the lipid species that is hydrophobically best matched (Jørgensen et al., 1993, 2000; Jørgensen and Mouritsen, 1995).

Submitted December 3, 2001, and accepted for publication March 20, 2002.

Address reprint requests to Roland Winter, University of Dortmund, Department of Chemistry, Physical Chemistry I, Otto-Hahn Strasse 6, D-44221 Dortmund, Germany. Tel.: 49-231-755-3900; Fax: 49-231-755-3901; E-mail: winter@steak.chemie.uni-dortmund.de.

0006-3495/02/07/334/11 $2.00

In the present paper we explore the effect of polypeptide incorporation on lipid lateral organization and concentration fluctuations and the possibility of molecular sorting of lipids by the embedded polypeptide, using a model membrane that is particularly suited to exploiting the effects of hydrophobic matching. The model system is the binary phospholipid mixture DMPC-DSPC (1:1 mol/mol) with acyl chains di-C_{14} (DMPC, dimyristoyl-phosphatidylcholine), and di-C_{18} (DSPC, distearoyl-phosphatidylcholine), and the incorporated polypeptide is gramicidin. The two lipid species have different hydrophobic chain lengths, which furthermore are each subjected to substantial changes with temperature because of their gel-to-fluid phase transition, which is accompanied by an average decrease of ~4 Å in lipid length due to the increase in the population of gauche conformers and kinks in the lipid acyl chains. In the gel phase, the hydrocarbon chains are in a straight, elongated conformation; in the fluid phase, they are conformationally disordered (chain melting transition). The large difference in hydrophobic length (4 CH_2 groups) of the two lipid species implies a strongly nonideal mixing behavior and, therefore, causes a broad two-phase coexistence region between the gel and all-fluid phase state (Mabrey and Sturtevant, 1976; Landwehr and Winter, 1994; Winter et al., 1999).

The region of interest in this study is the two-phase region. Measurements of fluorescence recovery after photobleaching have indicated the existence of highly heterogeneous gel and fluid domains in the coexistence region (Bultmann et al., 1991). Monte Carlo computer simulations of phase diagrams have exhibited long-lived percolation-like gel and fluid domains with a network of interfacial regions that have properties different from those of coexisting bulk phases (Jørgensen et al., 1993; Jørgensen and Mouritsen, 1995). Most recently, small-angle neutron diffraction (SANS) experiments with multilamellar vesicles have shown the presence of large-scale surface-fractal domains in the two-phase region (Czeslik et al., 1997; Winter et al., 1999). We interpreted the fluctuations as long-lived descendants of the incipient two-phase equilibrium state. These results also implied a variety of other unexpected properties of the two phases: contrary to expectations, the phase separation does not take place in each lipid bilayer independently, but produces gel and fluid domains correlated across many bilayers. Contrary to expectations, the amount and composition of the two phases differ strongly from those predicted by the equilibrium phase diagram. The data provided the first direct evidence that phase separation in multilamellar membranes is dominated by long-lived nonequilibrium structures, that these structures have ramified boundaries, and that their formation is governed by interlamellar interactions, outside the domain of single-bilayer statistical thermodynamics

Gramicidin, a pentadecapeptide antibiotic isolated from *Bacillus brevis*, is active against grampositive bacteria by forming membrane channels that are specific for monovalent cations, such as H^+ and alkali metals. Gramicidin A (GA) consists of alternating D- and L- amino acids in the sequence HCO-L-Val^1-Gly^2-L-Ala^3-D-Leu^4-L-Ala^5-D-Val^6-L-Val^7-D-Val^8-L-Trp^9-D-Leu^{10}-L-Trp^{11}-D-Leu^{12}-L-Trp^{13}-D-Leu^{14}-L-Trp^{15}-$NHCH_2CH_2OH$. Naturally occurring gramicidin, gramidicin D (GD), is a mixture of isoforms differing in amino acid composition at position 1, Val^1(VG)/Ile^1(IG), and position 11, Trp^{11}(GA)/Phe^{11}(GB)/Tyr^{11}(GC) (Burkhart et al., 1999; Sarges and Witkop, 1965), mainly consisting of GA (~80–85%). Gramicidin is one of the best-characterized transmembrane peptides and can adopt various conformations in different solvents (for a review, see Killian, 1992; Wallace, 1990). When incorporated into fluid lipid membranes, gramicidin forms monovalent cations channels in the form of a right-handed, single-stranded $\beta^{6.3}$ helical dimer (Arseniev et al., 1985; Cornell et al., 1988, 1989; Cross, 1997). The unusual primary structure has important consequences for the secondary structure and function of gramicidin. The peptide is able to adopt conformations of β-helices, which would be unacceptable for an all-L-amino acid peptide. The helices can be right- or left-handed, and they can differ in the number of amino acid residues per turn and, therefore, in length and diameter (Urry, 1971; Wallace, 1986, 1990, 1998; Killian, 1992; Koeppe and Andersen, 1996; Chadwick and Cardew, 1999). Individual gramicidin molecules can fold into single-stranded helices, which are stabilized by intramolecular hydrogen bonds, and can associate to helical dimers (HD) in which two single-stranded helices are joined end-to-end. Also, double-stranded helices (DH) can be formed in which the two strands run either parallel or antiparallel. Both, the double helix and helical dimer forms have β-sheet-like hydrogen bonding patterns, differing in the number of intra- and intermolecular hydrogen bonds and the helical rise per residue. The gramicidin monomers in β-type helical dimers are often found to have 6.3 residues per turn and an internal pore diameter of 3 to 4 Å, whereas the total length of the dimer is ~26 Å (Wallace, 1986, 1998). Double helices are found in organic solvents but also in lipid systems. At least four different types of double-helical structures have been found, such as left-handed antiparallel double helices with 5.6 residues per turn, being 36 Å long with a maximal lumen of 3 Å (Wallace, 1998; Veatch et al., 1974; Pascal and Cross, 1993; Langs et al., 1991; Burkhart et al., 1999).

To observe the heterogeneous membrane structure and lipid concentration fluctuations on a wide length scale, from nanometer to micrometer, SANS with H/D contrast variation (Czeslik et al., 1997; Winter et al., 1999) and two-photon excited fluorescence microscopy techniques were used (Bagatolli and Gratton, 2000a,b). The phase behavior and mesophase structure of the samples were determined using differential scanning calorimetry and small-angle x-ray scattering (SAXS). To determine how the membrane's lateral organization and phase state affects the gramicidin conformational state in the lipid bilayer, the amide I band

was analyzed using Fourier transform infrared (FTIR) spectroscopy (Zein and Winter, 2000).

MATERIALS AND METHODS

Materials and sample preparation

1,2-dimyristoyl-*sn*-glycero-3-phosphatidylcholine (DMPC) and 1,2-distearoyl-*sn*-glycero-3-phosphatidylcholine (DSPC) were purchased from Avanti Polar Lipids (Birmingham, AL) and GD from Sygena (Liestal, Switzerland). The chemicals were used without further purification.

Neutron small-angle scattering

Equimolar mixtures of DMPC(d_{54})/DSPC were prepared by dissolving the protonated and deuterated lipids in chloroform. The large difference in the coherent scattering length of hydrogen ($b_H = -0.374 \times 10^{-12}$ cm) and deuterium ($b_D = 0.667 \times 10^{-12}$ cm) provides an excellent contrast when one of the components is deuterated. The solvent was removed using a rotary evaporator, and the samples were lyophilized for several hours. Homogeneous samples consisting of multilamellar vesicles were obtained after several freeze-thaw-vortex cycles. The composition of the H_2O/D_2O mixture for the dispersion of the vesicles with a lipid mass fraction of ~30% was adjusted so that the scattering cross-section density of the solvent H_2O/D_2O was equal to that of a homogeneous mixture of the lipid components. Under these so-called matching conditions, scattering arises essentially from the inhomogeneous distribution of the lipid components in the vesicle.

Typically, for each temperature the measurements took 3 h. After a new temperature was adjusted, the sample was allowed to equilibrate for at least 15 min. To ensure that a new lamellar phase has indeed been formed within the time scale of the experiment and that the transitions are reversible, we recorded the lamellar *d*-spacings by small-angle x-ray diffraction (in-house Kratky camera system). The neutron scattering experiments were performed on the D11 diffractometer at the ILL in Grenoble and at the KWS2 diffractometer at the Forschungszentrum Jülich. The range of momentum transfers $Q = (4\pi/\lambda)\sin\Theta$ (scattering angle 2Θ, wavelength of radiation λ) was 2.5×10^{-3} to 1.5×10^{-1} Å^{-1}, covering a range of lengths ($2\pi/Q$) from 40 to 2500 Å. Standard treatment of isotropic SANS data was performed (Lindner and Zemb, 1991). The measured intensity distributions were corrected for absorption, sample thickness, inelasticity, and background.

Fluorescence microscopy

Vesicle preparation

LAURDAN (6-dodecanoyl-2-dimethylamino-naphthalene) and *N*-Rh-DPPE (Lissamine rhodamine B, 1,2-dihexadecanoyl-*sn*-glycero-3-phosphoethanolamine) were obtained from Molecular Probes (Eugene, OR). Stock solutions of phospholipids and GD were prepared in chloroform. The concentration of the lipid stock solutions was 0.2 mg/mL, the ratio DMPC/DSPC was 1:1 (mol/mol), and the ratio lipid/GD was 8:1 (w/w), corresponding to ~5 mol% GD. For giant unilamellar vesicles (GUV) preparations, we followed the electroformation method developed by Angelova and Dimitrov (Angelova and Dimitrov, 1986, 1987; Angelova et al., 1992). To grow the GUVs, a special temperature-controlled chamber, which was previously described (Bagatolli and Gratton, 1999), was used. The experiments were carried out in the same chamber after the vesicle formation, using an inverted microscope (Axiovert 35; Zeiss, Thornwood, NY). The following steps were used to prepare the GUVs: 1) 2 μL of the lipid solution was spread on each platinum (Pt) wire under a stream of N_2. To remove the residues of organic solvent the samples were lyophilized for 1 h. 2) To add the aqueous solvent inside the chamber (Millipore water 17.5 MΩcm), the bottom part of the chamber was sealed with a coverslip. The water was previously heated to 65°C and then sufficient water was added to cover the Pt wires. Just after this step the Pt wires were connected to a function generator (Hewlett-Packard, Santa Clara, CA), and a low-frequency AC field (sinusoidal wave function with a frequency of 10 Hz and an amplitude of 3 V) was applied for 90 min. After the vesicle formation, the AC field was turned off and the temperature scan (from high to low temperatures) was initiated. A CCD color video camera (CCD-Iris; Sony, Tokyo) in the microscope was used to follow vesicle formation and to select the target vesicle. The temperature was measured inside the sample chamber with a digital thermocouple (model 400B; Omega, Stamford, CT) with a precision of 0.1°C. The fluorescent probes were premixed with the lipids in chloroform (the LAURDAN/lipid ratio is 1:50 (mol/mol), taking into account the dilute lipid concentration and the partition coefficient of LAURDAN, the actual LAURDAN/lipid ratio in the lipid vesicle is known to be much lower; the *N*-Rh-DPPE/lipid ratio is 1:100 (mol/mol)).

Generalized polarization function

The emission spectrum of LAURDAN is blue in the lipid gel phase, whereas in the liquid-crystalline phase it moves during the excited-state lifetime from the blue to the green (Parasassi et al., 1997 and references therein). To quantify the emission spectral changes, the excitation generalized polarization (GP) function was defined analogously to the fluorescence polarization function as

$$\mathrm{GP} = \frac{I_B - I_R}{I_B + I_R} \tag{1}$$

in which I_B and I_R correspond to the intensities at the blue and red edges of the emission spectrum, respectively, for a given excitation wavelength.

Experimental apparatus

The two-photon excitation microscopy experiments were performed at the Laboratory of Fluorescence Dynamics (University of Illinois at Urbana-Champaign). The high photon densities required for two-photon absorption are achieved by focusing a high peak power laser light source on a diffraction-limited spot through a high numerical aperture objective. Therefore, in the areas above and below the focal plane, two-photon absorption does not occur because of insufficient photon flux. This phenomenon allows a sectioning effect without the use of emission pinholes as in confocal microscopy. Another advantage of two-photon excitation is the low extent of photobleaching and photodamage above and below the focal plane. For our experiments, we used a scanning two-photon fluorescence microscope (So et al., 1995, 1996). For the LAURDAN GP measurements we used a procedure similar to that previously described (Yu et al., 1996; Parasassi et al., 1997; Bagatolli and Gratton, 1999). We used an LD-Achroplan 20× long working distance air objective (Zeiss, Homldale, NJ) with a numerical aperture of 0.4. A titanium-sapphire laser (Mira 900; Coherent, Palo Alto, CA) pumped by a frequency-doubled Nd:vanadate laser was used as the excitation light source. The excitation wavelength was set at 780 nm. The laser was guided by a galvanometer-driven *x*-*y* scanner (Cambridge Technology, Water-Town, MA) to achieve beam scanning in both the *x* and *y* directions. The scanning rate was controlled by the input signal from a frequency synthesizer (Hewlett-Packard, Santa Clara, CA), and a frame rate of 25 s was used to acquire the images (256 × 256 pixels). To change the polarization of the laser light from linear to circular, a quarter wave plate (CVI Laser Corporation, Albuquerque, NM) was placed after the polarizer. The fluorescence emission was observed through a broad band-pass filter from 350 to 600 nm (BG39 filter; Chroma Technology, Brattleboro, VT). For measuring LAURDAN GP values, two additional optical band-pass filters with 46-nm width and centered at 446 nm and at 499 nm (Ealing Electro-Optics, New Englander Industrial Park, Holliston, MA) were used to collect fluorescence in the blue and green

regions of LAURDAN′s emission spectrum, respectively. A miniature photomultiplier (R5600-P; Hamamatsu, Brigdewater, NJ) was used for light detection in the photon counting mode. A home-built card in a personal computer acquired the counts. GP values were corrected for the different transmission properties of the optical filters by using a solution of Laurdan in dimethyl sulfoxide.

FTIR measurements

The GD-lipid mixtures were prepared by codissolving the components in chloroform, vortex mixing the solution in sealed containers, and drying the solution under vacuum. The samples were then kept under vacuum for at least 16 h. Fully hydrated (80 wt% D_2O) gramicidin-lipid bilayer dispersions were prepared for the infrared experiments by heating the hydrated mixtures in a closed vessel to a temperature well above the gel to liquid-crystalline phase transition temperature, vortex mixing the heated samples, and freezing the samples in liquid nitrogen. This freeze-thaw cycle was repeated five times to ensure equilibration of gramicidin in the lipid bilayer and to obtain homogeneous lipid dispersions.

The lipid dispersions were filled into a 25-μm-thick infrared cell with CaF_2 windows. To achieve thermal equilibrium, a 20-min wait was adopted at each new temperature before data were taken. Infrared spectra were collected on a Nicolet Magna 550 FTIR spectrometer (Thermo Nicolet, Offenbach) with a liquid nitrogen-cooled cadmium telluride detector. For each spectrum 256 interferograms were co-added at a spectral resolution of 2 cm^{-1} and apodized with a Happ-Genzel function. The sample chamber was purged with dry, carbon dioxide-free air during data collection to minimize spectral contributions from atmospheric gases. All of the data analysis, including determination of the vibrational frequencies, was done with the OMNIC software developed by Nicolet Instruments (Thermo Nicolet, Offenbach).

The amide I′ mode of gramicidin appears in the spectral range from 1700 to 1600 cm^{-1} and may result of overlapping absorption bands of different frequencies, intensities, and half-widths, which belong to a particular type of secondary structure of gramicidin (Naik and Krimm, 1986a,b; Bandekar, 1992). The fractional intensities of the secondary elements were calculated from band-fitting procedures assuming a Gaussian-Lorentzian lineshape function (Byler and Susi, 1986). The bands associated with particular types of secondary structure elements were determined by Naik and Krimm (1986) using normal mode calculations. Forth derivative and Fourier self-deconvolution of the spectra led to the identification of subbands. We analyzed spectral changes in the amide I band region following the absorption bands occurring at ~1631 and 1646 to 1648 cm^{-1}, which are expected to originate from the single-stranded helical dimers $\beta^{4.4}$ [HD(1)] and $\beta^{6.3}$ [HD(2)], respectively, and at ~1636, 1656, and 1666 to 1669 cm^{-1}, which originate from double-stranded antiparallel and parallel double-stranded $\beta^{5.6}$ helices (DH) (Naik and Krimm, 1986). In several papers, a single band around 1631 cm^{-1} has been assigned to a $\beta^{6.3}$ helical dimer structure. This assignment is based on the corresponding CD spectra, however (Bouchard and Auger, 1993; Sychev et al., 1993), and a single-stranded, right-handed channel conformation of GA with ~6.5 residues per turn (5.1-Å helical pitch) forming a 4-Å diameter pore in fluid DMPC bilayers has been determined using solid-state nuclear magnetic resonance spectroscopy (Cornell et al., 1988; Kovacs et al., 1996; Quist, 1998). It might as well be that the 6.3 and 4.4 helical dimer structures are just slightly different forms of single stranded dimers. Future normal mode calculations might help to solve this problem. Owing to these current uncertainties in conformer assignment we denote the two helical dimer states as HD(1) and HD(2), respectively. The bands assigned to different conformers might have different transition dipole moments, so the fractional intensities do not correspond directly to concentrations.

RESULTS

Characterization of DMPC-DSPC/GD samples

Differential scanning calorimetry, FTIR, and SAXS data have shown that the gel-fluid coexistence region of the pure equimolar lipid mixture DMPC-DSPC appears between ~30°C and 49°C (Winter et al., 1999 and references therein). Deuteration of one lipid component lowers both temperatures by ~4°C. Hence, above 45°C a fluid-like liquid-crystalline phase is observed in DMPC(d_{54})-DPSC dispersions and below 26°C an all-gel phase appears. The phase diagram observed for DMPC-DSPC and the partially deuterated DMPC-DSPC mixture is in good agreement with that based on other experimental or theoretical data (Mabrey and Sturtevant, 1976; Sankaram and Thompson, 1992; Morrow et al., 1991; Jørgensen and Mouritsen, 1995; Leidy et al., 2001). A peritectic phase behavior with gel-gel phase coexistence, associated three-phase line, and a critical lateral demixing behavior as observed by Knoll et al. (1981, 1983, 1991) has not been seen in these measurements.

Incorporation of 2 to 5 mol% GD into the DMPC-DSPC bilayer system leads to a decrease of the width of the gel-fluid two-phase region and at low temperatures a gel-gel coexistence region occurs. For example, for the sample DMPC-DSPC/5 mol% GD the phase sequence gel-gel/gel/gel-fluid/fluid has been determined using SAXS and FTIR spectroscopy, where the gel-gel to gel transition occurs around 26°C, and the gel-fluid coexistence region appears between 38°C and 48°C only. The SAXS data reveal that low GD concentrations (<2 mol%) cause a drastic swelling of the lipid bilayer system in its all gel phase. The lamellar lattice constant d in the gel phase of the lipid mixture increases from ~68 to ~80 Å. The gel-gel two-phase region is indicated by two first-order lamellar Bragg reflections below 26°C, corresponding to lamellar d-spacings of 56 and 76 Å, respectively. A similar behavior is observed for the DMPC-DSPC/2 mol% GD mixture. Here, the gel-fluid coexistence region appears between 32°C and 49°C. In the all-fluid phase of DMPC-DSPC/GD samples, the lamellar lattice constants of all samples are similar ($d \approx 68$ Å).

Neutron small-angle scattering

The differential scattering cross-section per unit volume of the samples can be written as (Brumberger, 1995)

$$\frac{d\Sigma}{d\Omega} = n_p(\Delta\rho)^2 V_p^2 P(Q)S(Q), \qquad (2)$$

in which n_p denotes the number density of particles (lipid molecules), V_p the particle volume, and $\Delta\rho = \rho_p - \rho_s$ the contrast, i.e., the difference in mean scattering length density of the particles (ρ_p) and the solvent (ρ_s). $P(Q)$ is the form factor of the particles, and $S(Q)$ is the structure factor describing the spatial distribution of the particles. By setting $P(Q) = 1$, we

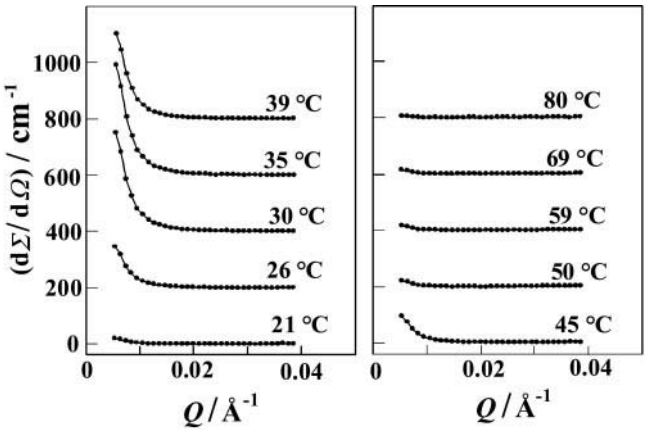

FIGURE 1 SANS curves of a DMPC(d_{54})-DSPC aqueous dispersion in excess water at mole fraction $x_{DSPC} = 0.5$. The curves at different temperatures are shifted by 200 cm^{-1} relative to each other.

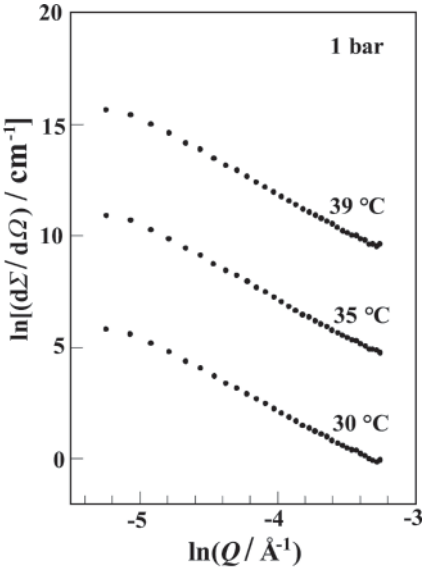

FIGURE 2 Ln-ln plots of selected SANS curves of the DMPC(d_{54})-DSPC dispersion in Fig. 1, shifted by $\ln[d\Sigma/d\Omega\ (cm^{-1})] = 5$.

treat the molecules as point particles and the sample as consisting of two phases, each of which has a constant scattering length density described by $S(Q)$. This treatment is appropriate because we analyze data only at $Q < 0.03$ $Å^{-1}$.

As mentioned above, deuteration of DMPC lowers the transition of DMPC by 4°C and shifts the two-phase region of DMPC(d_{54})/DSPC to 26°C to 45°C. Fig. 1 shows the SANS curves of the mixture for the temperature range between 21°C and 80°C. As can be clearly seen, almost zero scattering intensity is observed at low and high temperatures, in the all-gel and fluid phase region, respectively, as expected for a homogeneous mixture of the two lipid components, which leads to $\Delta\rho = 0$ (see Eq. 2). The scattering intensity increases significantly in the two-phase region. No Porod slope of -4 is observed at large Q-values ($S(Q) = 2\pi A_s/Q^4$, with A_s the total surface area), at which the intensity is governed by the small-scale surface structure of the scatterer (Brumberger, 1995). This shows that the objects (fluctuation geometries) giving rise to the observed scattering do not have smooth surfaces.

The $\ln(d\Sigma/d\Omega)$ versus $\ln(Q)$ plot gives a straight line over the whole Q-range covered (Fig. 2), i.e., over distances ranging from ~200 Å to 1500 Å. Such a power-law scattering is indicative of a fractal-like behavior of the sample. When irregular structures are involved, the concept of fractal geometry is often used as a quantitative measure of the space-filling properties of the system (Pfeifer and Obert, 1989). For fractal objects in three dimensions that are self-similar over a range of length scales, the structure factor is:

$$S(Q) = 1 + \frac{1}{(Qa)^{D_m}} \cdot \frac{D_m \Gamma(D_m - 1)}{(1 + 1/Q^2\xi^2)^{(D_m-1)/2}} \times \sin[(D_m - 1)\arctan(Q\zeta)] \quad (3)$$

in which $\Gamma(x)$ is the gamma function, and D_m is the fractal dimension of the object (mass fractal), which relates the size r of the object to its total mass ($m \propto r^{D_m}$, $0 < D_m < 3$). Eq. 3 reduces to $S(Q) \propto Q^{-D_m}$ when $\xi^{-1} < Q < a^{-1}$. ξ is the cutoff distance of the fractal object, and a is the characteristic size of the individual scatterers. For scattering from three-dimensional objects with fractal surface (surface fractals), having the property that the surface area varies as a noninteger power of length, the power law exponent is $-(6 - D_s)$, in which D_s is the fractal dimension of the surface ($2 \le D_s < 3$). $D_s = 2$ represents a smooth surface. From the log-log plot in Fig. 2, a slope of -3.1 ± 0.1 is obtained, which yields a surface fractal dimension of $D_s = 2.9 \pm 0.1$. The absence of a cross-over at both ends of the power-law regime gives $a < 240$ Å and $\xi > 1200$ Å.

Fig. 3 exhibits the SANS curves for DMPC/DSPC mixtures with different concentrations of GD for example at $T = 40$°C, i.e., at a temperature within the gel-fluid two-phase region of all samples. As can be clearly seen, the incorporation of the polypeptide leads to a drastic decrease of concentration fluctuations. Addition of 2 mol% GD causes an ~50% decrease of the small-angle scattering intensity. A power-law scattering with an exponent of -3.0 ± 0.2 is observed in the two-phase region (Fig. 4). Compared with the pure binary lipid system, medium-sized concentration fluctuations (at $\xi \approx 600$ Å) occur about a factor of two more frequently than concentration fluctuations of larger correlation length (at $\xi \approx 1200$ Å). Incorporation of 5 mol% GD leads to a further decrease of the concentration fluctuations (~90%–100% relative to the pure lipid mixture) and the exponent from the log-log plot is -3.3 ± 0.1, again consistent with surface-fractal fluctuations of dimension $D_s = 2.7 \pm 0.1$. This decrease in concentration fluctuations is accompanied by an increase of the lower limit of correlation lengths: $\xi > 240$ Å for the

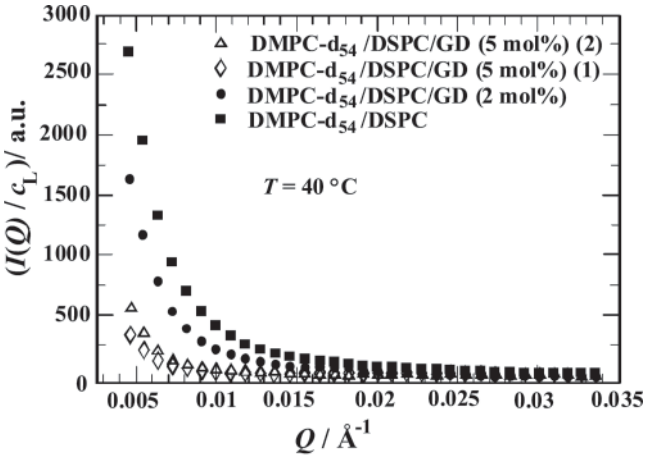

FIGURE 3 SANS curves $I(Q)$ of a DMPC(d_{54})-DSPC (1:1 mol/mol) mixture with different GD concentrations at $T = 40$°C. For the sample with 5 mol% GD, SANS data for two matching conditions are shown: (1) lipids matched only, (2) lipids and GD matched. The intensity data are normalized to the phospholipid concentration c_L (Hunt et al., 1997).

pure lipid mixture, $\xi > 370$ Å for DMPC/DSPC/2 mol% GD, and $\xi > 450$ Å for the lipid dispersion with 5 mol% GD.

For the sample DMPC/DSPC/5 mol% GD, the scattering contrast was varied so as to match the mean scattering length density of the binary lipid mixture and the whole sample including GD. No significant differences were observed (Fig. 3), however, indicating that the small-angle scattering is dominated by the concentration fluctuations of the lipid species and no significant polypeptide aggregation seems to occur. Indeed, a slight increase in the scattering intensity of the totally matched sample is observed, pointing to the fact that the protein scattering length density partially compensates the scattering contribution of the gel/fluid domains with their different concentrations of hydrogenated and deuterated lipid components.

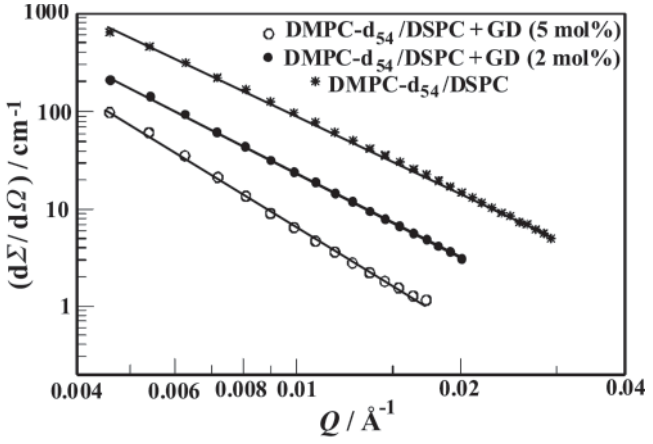

FIGURE 4 Ln-ln plots of the SANS curves of DMPC(d_{54})-DSPC mixtures without and with different GD concentrations at $T = 40$°C.

Fluorescence microscopy

Fluorescence microscopy was used for direct visualization of the lateral lipid organization providing information of lipid domain shapes on a micrometer length scale including information about the lipid phase state. GUV of the lipid mixtures were prepared that could be observed under the two-photon excitation fluorescence microscope. Two different fluorophores were used, Laurdan and *N*-Rh-DPPE. The fluorophore Laurdan is homogeneously distributed between the gel and fluid lipid phases. From the Laurdan intensity images, the excitation GP function was calculated (Eq. 1) to characterize the phase state of the lipid domains. In the case of *N*-Rh-DPPE, the different probe partitioning between gel and fluid domains discriminates between fluid and gel-state domains.

DMPC-DSPC

In the fluid phase of the lipid bilayer system the images obtained with *N*-Rh-DPPE show that the fluorescent molecules are distributed homogeneously on the vesicle surface (Fig. 5 *A*). As the temperature was decreased to the gel-fluid two-phase region, nonfluorescent areas become visible on the vesicle surface showing lipid domain coexistence (Fig. 5, *B* and *C*). The lipid gel-type domains expand and migrate around the vesicle surface as we decrease the temperature. The gel-type domains span the inner and outer leaflets of the membrane, suggesting a strong coupling between the inner and outer monolayer of the lipid bilayer. Below 30°C, the nonfluorescent regions disappear again, showing an essentially homogeneous fluorescence distribution on the vesicle surface.

The Laurdan GP images of DMPC-DSPC vesicles at four different temperatures are shown in Fig. 6, *A* through *D*. In GUVs in the fluid phase (Fig. 6 *A*), a homogeneous distribution of GP values is obtained with values of approximately -0.1. Reaching the phase coexistence region, the GP images show a separation between GP values typical of fluid and gel-type domains, -0.1 and 0.5, respectively (Fig. 6, *B* and *C*). In this case, the LAURDAN GP histogram is bimodal (Fig. 7, *B* and *C*). The center of the fluid and solid components of the GP histograms in the phase coexistence region are similar to those obtained in the fluid and gel temperature regions of the mixture (Fig. 6, *A* and *D*). Below the gel-fluid phase transition region, the GP image is homogeneous again with GP values of ~ 0.55, which are characteristic for a gel-type lipid phase state.

DMPC-DSPC/GD

Images in the fluid phase of the lipid mixture with 5 mol% GD and *N*-Rh-DPPE as fluorophore show a homogeneous distribution of fluorescent molecules on the vesicle surface like in the case without gramicidin (Fig. 5 *D*). With decreas-

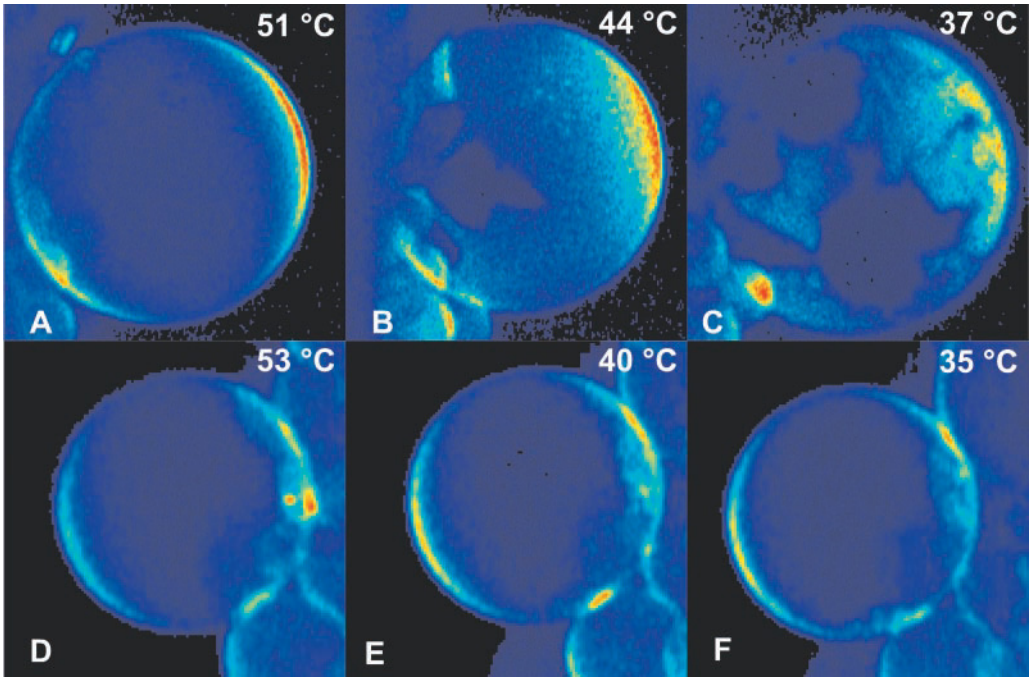

FIGURE 5 Two-photon excitation fluorescence intensity spectra (false color representation) of GUVs (size ~30 μm) formed of DMPC-DSPC (*A–C*) and DMPC-DSPC/5 mol% GD dispersions (*D–F*), labeled with *N*-Rh-DPPE. The images were taken at the top part of the GUVs at temperatures corresponding to the fluid phase (*A*, *D*), gel-fluid phase coexistence region (*B*, *C*, *E*), and gel phase (*F*).

ing temperature, no nonfluorescent areas become visible in the GD containing sample, however (Fig. 5, *E* and *F*). This means that no significant domain coexistence with domain sizes in the micrometer range occurs in the gel-fluid coexistence region. The corresponding Laurdan GP images and GP histograms are shown in Fig. 6, *E* to *H* and Fig. 7, *E* to *H*. In the fluid phase there is no difference to the GP image and histogram of the sample without GD (Figs. 6 *E* and 7 *E*). Lowering the temperature leads to a continuous change in the GP values (Fig. 6, *F* and *G*) until the gel-phase is reached (Fig. 6 *H*). In the whole temperature range the GP histogram is unimodal (Fig. 7, *E–H*). No regions of strongly different GP values can be observed in the Laurdan GP images. These data clearly indicate that incorporation of GD also leads to drastic changes of concentrations fluctuations at micrometer length scales.

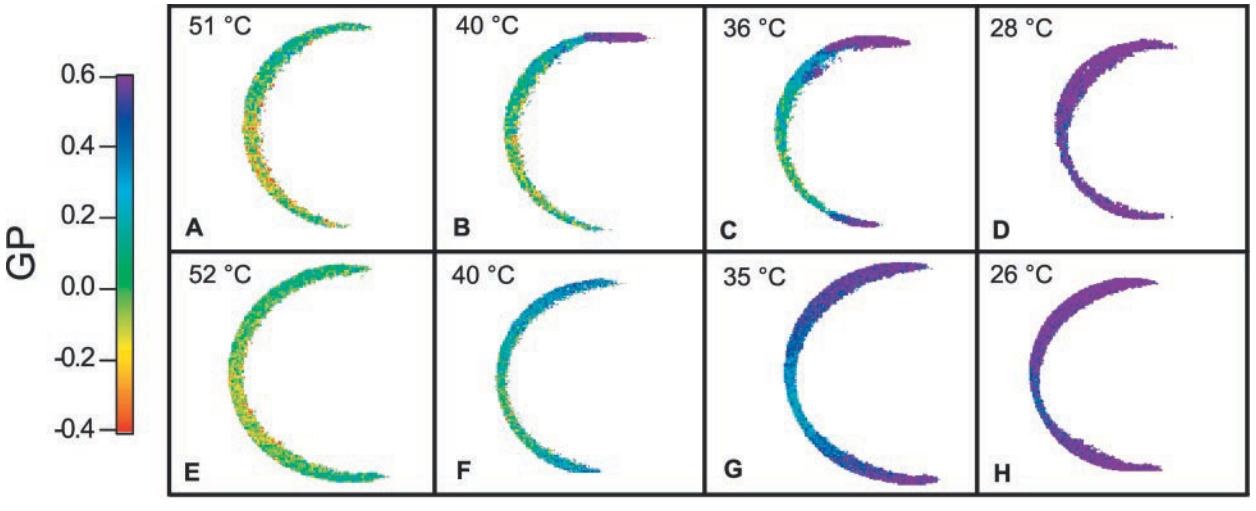

FIGURE 6 Two-photon Laurdan GP images of a single GUV (size ~30 μm) composed of DMPC-DSPC (*A–D*) and DMPC-DSPC/5 mol% GD (*E–H*) obtained with circular polarized light. The images were taken at the equatorial region of the vesicle at temperatures corresponding to the fluid phase (*A*, *E*), gel-fluid phase coexistence region (*B*, *C*, *F*, *G*), and gel phase (*D*, *H*).

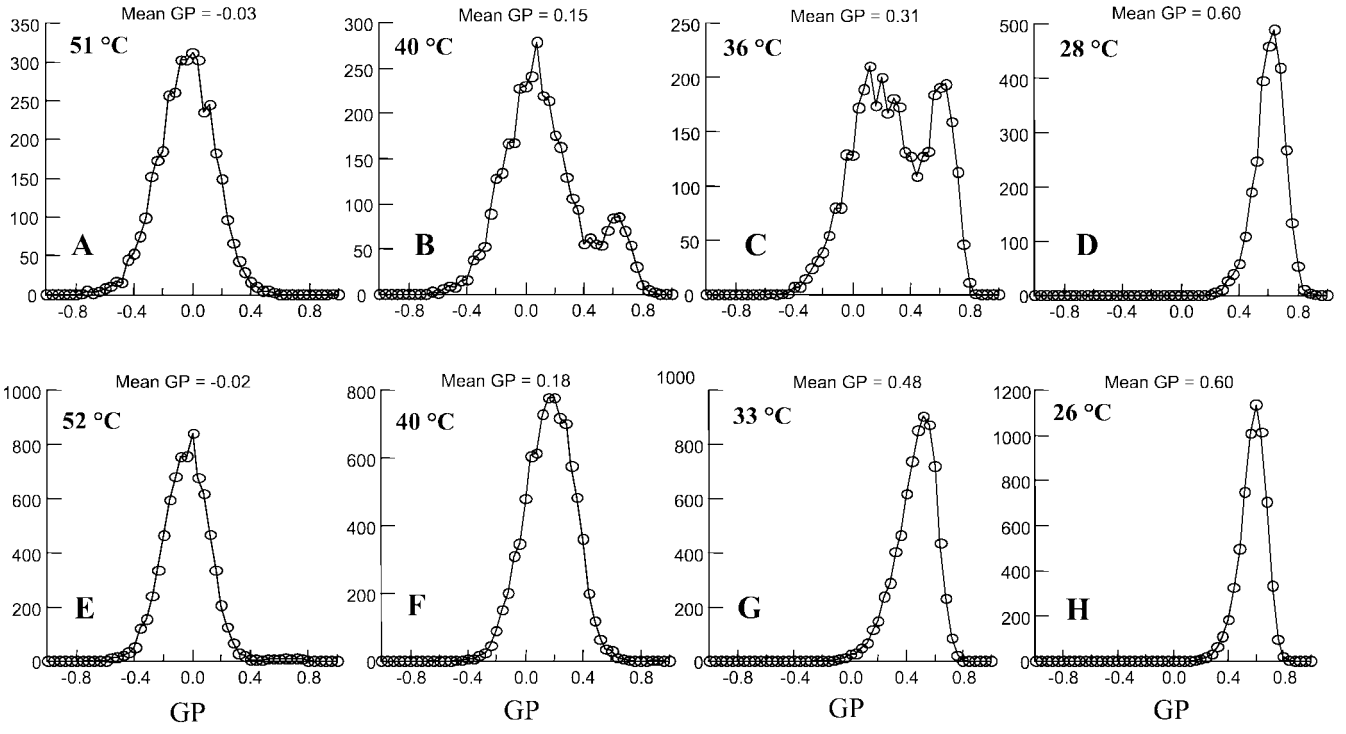

FIGURE 7 Laurdan GP histograms of single GUV composed of DMPC-DSPC (*A–D*) and DMPC-DSPC/5 mol% GD (*E–H*) corresponding to the images presented on Fig. 6. The images were taken at temperatures corresponding to the fluid phase (*A*, *E*), gel-fluid phase coexistence region (*B*, *C*, *F*, *G*), and gel phase (*D*, *H*).

Infrared spectroscopy

DMPC-GD and DSPC-GD

In a previous work we studied the conformation of GD in one-component lipid bilayer systems, such as DMPC and DSPC, using FTIR spectroscopy (Zein and Winter, 2000). The maximum of the amide I′ band of the DMPC-GD sample containing 5 mol% GD is located at ~1632 cm^{-1} and the band exhibits a broad shoulder on the high frequency side (data not shown) (Zein and Winter, 2000). With increasing temperature there is no significant change in wave number or in shape of the amide I′ band. The temperature dependence of the fractional intensities of the secondary structural elements obtained using the normal mode calculation from Naik and Krimm (1986) is shown in Fig. 8. We find that gramicidin in DMPC can adopt different types of secondary structures, helical dimers, and double helices. The equilibrium of the gramicidin species in the DMPC-GD (5 mol %) mixture seems to be in favor of HD conformations. We cannot give quantitative numbers owing to the unknown IR transition dipole moments of the different conformers, however. The data clearly indicate that no significant change in the conformational behavior of gramicidin occurs within the measured temperature range. Above ~27°C, only a very small change in fractional intensities is observed. As indicated by differential scanning calorimetry measurements (data not shown), below ~28°C a broad gel-fluid co-existence region occurs in the DMPC-GD (5 mol%) mixture. Above that temperature, the lipid is in an all-fluid-like phase.

The position of the amide I′ band maximum of DPSC/5 mol% GD is shifted to lower frequencies above 41°C and remains constant above 56°C. In Fig. 9, the fractional intensities of the different gramicidin conformers are shown as a function of temperature. In the temperature range from

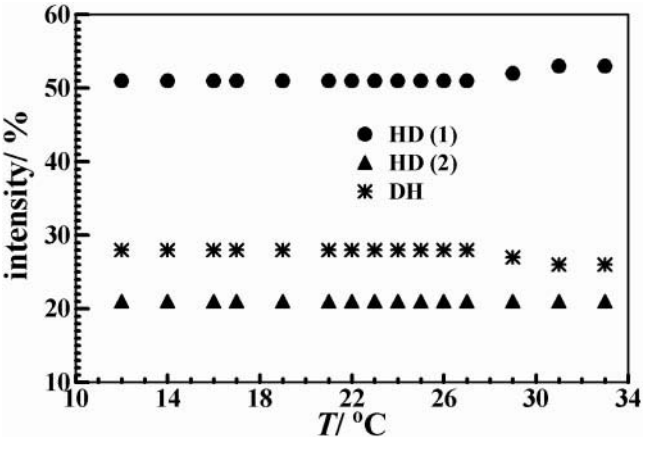

FIGURE 8 Temperature dependence of the IR fractional band intensities of gramicidin conformations in DMPC/GD (5 mol%) (HD single-stranded helical dimers, DH double helix conformation).

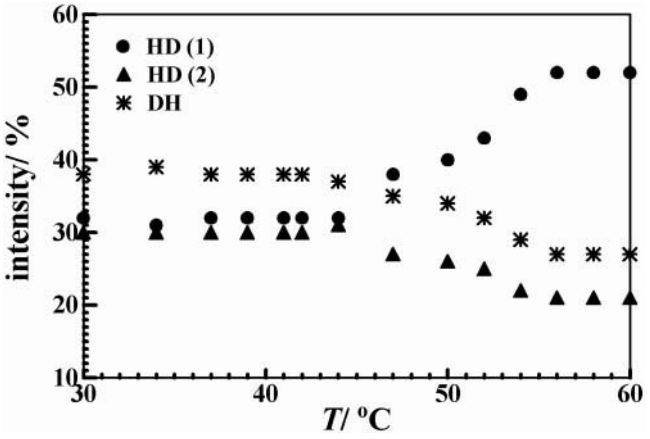

FIGURE 9 Temperature dependence of the IR fractional band intensities of gramicidin conformations in DSPC/GD (5 mol%) (HD single-stranded helical dimers, DH double helix conformation).

20°C to ~40°C the fractional intensities of the different species remain constant. The equilibrium conformation in the low temperature region is in favor of the double helix. When the temperature is increased above 40°C, the fractional intensity of HD(1) increases with a concomitant decrease in the fractional intensities of both other species. The equilibrium of the gramicidin conformations is shifted in favor of the HD(1) species at high temperature. The HD conformations turn out to be the main component in all saturated phospholipid fluid phases observed.

DMPC-DSPC/GD

In Fig. 10, the fractional intensities of the different gramicidin conformers are shown as a function of temperature for the system DMPC-DSPC/5 mol% GD. As can be clearly seen, the fractional intensities of the different species remain essentially constant. Contrary to the DSPC/5 mol% GD lipid bilayer system, also in the gel phase of DMPC-DSPC with 5 mol% GD the HD conformations seem to prevail. Similar results were obtained for the binary lipid system containing 2 mol% GD.

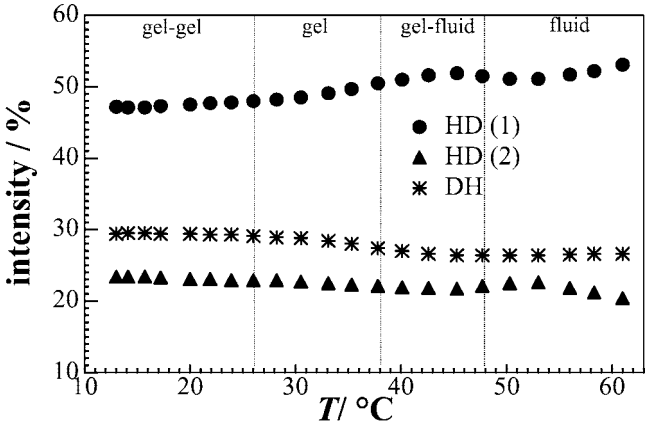

FIGURE 10 Temperature dependence of the IR fractional band intensities of gramicidin conformations in DMPC-DSPC (1:1 mol/mol)/GD (5 mol%).

These findings can be understood assuming that the polypeptide prefers to partition into DMPC-rich domains adopting a HD conformation. A slight increase in the HD population is observed at the gel-gel to gel phase transition temperature of ~26°C. At that temperature a decrease in the DSPC chain length due to an increase in lipid tilt angle and/or increase of population of non-all *trans* conformational states might lead to the observed formation of slightly more HD states at the expense of DH structures, possibly via a zipper type of mechanism, in which the monomer chains are proposed to unscrew in opposite directions in sequential steps.

DISCUSSION AND CONCLUSIONS

The data clearly show that gramicidin insertion has a significant influence on the lipid bilayer structure and temperature dependent phase behavior. To avoid large hydrophobic mismatch, the lipid conformation and lateral organization is altered. But also the conformational state of the embedded polypeptide is modulated by the lipid matrix. The gramicidin conformers differ in the number of amino acid residues per turn and, therefore, in length. The lengths have been found to be ~24 Å for the dimeric single-stranded right-handed $\beta^{6.3}$-helix and ~36 Å for the left-handed antiparallel double-stranded $\beta^{5.6}$-helix. For the $\beta^{4.4}$-helix no experimental data are available so far, its length will be greater than that of the dimeric $\beta^{6.3}$-helix, however. For comparison, the hydrophobic fluid bilayer thicknesses are ~28 and 32 Å for DMPC and DSPC bilayers, respectively (Gil et al., 1998). The hydrophobic thicknesses of the gel phases are 4 to 5 Å larger. Hydrophobic matching, in which transmembrane proteins cause the surrounding lipid bilayer to adjust its hydrocarbon thickness to match the length of the hydrophobic surface of the protein, is a commonly accepted idea in membrane biophysics and is also expected to influence the conformer population in our systems (Harroun et al., 1999a,b).

We have seen that the lipid matrix has the ability to modulate the conformation of the inserted polypeptide. The balance between DH and HD structures depends on the phospholipid hydrocarbon chain length and phase state. In DMPC bilayers, HD folds are the most prominent conformational states, but the double-helix form is also found. Owing to its unknown IR transition dipole moment, its concentration may be low, however. The change in phase state has only a very small effect on the population ratio of the conformers. In DSPC lipid bilayers, the population of DH forms increases in the gel state, the HD is abundant at high temperature. Owing to the formation of broad fluid-gel phase co-existence regions, a continuous change in the

population ratio is observed for the intermediate temperature regions. Destabilization of the HD conformation in the thicker DSPC gel phase membranes is probably related to the hydrophobic mismatch between lipid length and polypeptide hydrophobic surface. The changes observed might be attributed, at least partially, to the ability of the double helical conformation to tolerate more hydrophobic mismatch than the helical dimer, perhaps owing to an increased number of stabilizing intermolecular hydrogen bonds.

Contrary to the DSPC/5 mol% GD lipid bilayer system, also in the gel phase of DMPC-DSPC with 5 mol% GD the HD conformations prevail. This finding can be understood assuming that the polypeptide prefers to partition into DMPC-rich domains adopting a HD conformation. In the binary lipid systems not only in the gel-fluid phase-separated regions but also in the all-gel phases, interfacial adsorption phenomena and a molecular sorting mechanism, i.e., a selective accumulation of lipid species (here DMPC) that hydrophobically match the protein surface, seem to be operative. As a further consequence, in the gel-fluid coexistence region of the lipid bilayer system the gel-fluid domain size distribution is expected to change. Here we observe a drastic decrease in the domain size and concentration fluctuations of nanometer to micrometer size in the GD containing binary lipid system. For example, incorporation of 2 mol% GD leads to a ~50% decrease of the concentration fluctuations, and this decrease is accompanied by an increase of the lower limit their correlation length ($\xi > 240$ Å for the pure lipid mixture, $\xi > 370$ Å for DMPC/DSPC/2 mol% GD) and a relatively more pronounced damping of the concentration fluctuations at length scales above ~1000 Å.

To conclude, first, the molecular lipid environment has a considerable influence on the polypeptide conformer stability and structure, and, therefore, the choice of a membrane mimetic environment is an important issue that should not be neglected in membrane biophysical studies on model biomembrane systems. Second, the lateral lipid organization and domain size distribution is significantly influenced by the incorporation of the polypeptide into the lipid bilayer system via a molecular sorting mechanism.

We thank Dr. G. Meier for assistance with the SANS experiments in Jülich. We gratefully acknowledge financial support from the Deutsche Forschungsgemeinschaft and the Fonds der Chemischen Industrie. We wish to thank the Laboratory of Fluorescence Dynamics (LFD), University of Illinois at Urbana/Champaign for the opportunity to carry out two-photon fluorescence microscopy measurements. The LFD is supported jointly by the Division of Research Resources of the National Institutes of Health (PHS 5 P41-RRO3155) and University of Illinois at Urbana/Champaign.

REFERENCES

Angelova, M. I., and D. S. Dimitrov. 1986. Liposome electroformation. *Faraday Discuss. Chem. Soc.* 81:303–311.

Angelova, M. I., S. Soléau, Ph. Meléard, J. F. Faucon, and P. Bothorel. 1992. Preparation of giant vesicles by external AC fields: kinetics and application. *Prog. Colloid Polym. Sci.* 98:127–131.

Arseniev, A. S., I. L. Barsukov, V. F. Bystrov, A. L. Lomize, and Y. A. Ovchinnikov. 1985. ^{1}H-NMR study of gramicidin A transmembrane ion channel: head-to-head right-handed, single-stranded helices. *FEBS Lett.* 186:168–174.

Bagatolli, L. A., and E. Gratton. 1999. Two-photon fluorescence microscopy observation of shape changes at the phase transition in phospholipid giant unilamellar vesicles. *Biophys. J.* 77:2090–2101.

Bagatolli, L. A., and E. Gratton. 2000a. Two photon fluorescence microscopy of coexisting lipid domains in giant unilamellar vesicles of binary phospholipid mixtures. *Biophys. J.* 78:290–305.

Bagatolli, L. A., and E. Gratton. 2000b. A correlation between lipid domain shape and binary phospholipids mixture composition in free standing bilayers: a two-photon fluorescence microscopy study. *Biophys. J.* 79: 434–447.

Bandekar, J. 1992. Amide modes and protein conformation. *Biochim. Biophys. Acta.* 1120:123–143.

Bouchard, M., and M. Auger. 1993. Solvent history dependence of gramicidin-lipid interactions: a Raman and infrared spectroscopic study. *Biophys. J.* 65:2484–2492.

Brumberger, H. 1995. Modern Aspects of Small-Angle Scattering. Kluwer Academic Publishers, Dordrecht, The Netherlands.

Bultmann, T., W. L. C. Vaz, E. C. C. Melo, R. B. Sisk, and T. E. Thompson. 1991. Fluid-phase connectivity and translational diffusion in an eutectic, two-component, two-phase phosphatidylcholine bilayer. *Biochemistry.* 30:5573–5579.

Burkhart, B. M., R. M. Gassman, D. A. Langs, W. A. Pangborn, W. L. Duax, and V. Pletnev. 1999. Gramicidin D conformation, dynamics and membrane ion transport biopolymers. *Biopolymers.* 51:129–144.

Byler, D. M., and H. Susi. 1986. Examination of the secondary structure of proteins by deconvolved FTIR spectra. *Biopolymers.* 25:469–487.

Chadwick, D. J., and G. Cardew, editors. 1999. Gramicidin and Related Ion Channel-Forming Peptides. Novelties Foundation Symposium 225. John Wiley and Sons, New York.

Cornelius, F. 2001. Modulation of Na, K-ATPase and Na-ATPase activity by phospholipids and cholesterol: I. Steady-state kinetics. *Biochemistry.* 40:8842–8851.

Cornell, B. A., F. Separovic, A. J. Baldassi, and R. Smith. 1988. Conformation and orientation of gramicidin A in oriented phospholipid bilayers measured by solid-state carbon-13 NMR. *Biophys. J.* 53:67–76.

Cornell, B. A., F. Separovic, D. E. Thomas, A. R. Atkins, and R. Smith. 1989. Effect of acyl chain length on the structure and motion of gramicidin A in lipid bilayers. *Biochim. Biophys. Acta.* 985:229–232.

Cross, T. A. 1997. Solid-state nuclear magnetic resonance characterization of gramicidin channel structure. *Methods Enzymol.* 289:672–696.

Curran, A. R., R. H. Templer, and P. J. Booth. 1999. Modulation of folding and assembly of the membrane protein bacteriorhodopsin by intermolecular forces within the lipid bilayer. *Biochemistry.* 38:9328–9336.

Czeslik, C., J. Erbes, and R. Winter. 1997. Lateral organization of binary-lipid membranes: evidences for fractal-like behavior in the gel-fluid coexistence region. *Europhys. Lett.* 37:577–582.

Davies, S. M. A., R. M. Epand, R. Kraayenhof, and R. B. Cornell. 2001. Regulation of CTP: phosphocholine cytidylyltransferase activity by the physical properties of lipid membranes: an important role for stored curvature strain energy. *Biochemistry.* 40:10522–10531.

Dimitrov, D. S., and M. J. Angelova. 1987. Lipid swelling and liposome formation on solid surfaces in external electric fields. *Prog. Colloid Polym. Sci.* 73:48–56.

Dumas, F., M. M. Sperotto, M.-C. Lebrun, J.-F. Tocanne, and O. G. Mouritsen. 1997. Molecular sorting of lipids by bacteriorhodopsin in dilauroylphosphatidylcholine/distearoylphospha-tidylcholine lipid bilayers. *Biophys. J.* 73:1940–1953.

Estrela-Lopis, I., G. Brezesinski, and H. Möhwald. 2000. Influence of model membrane structure on phospholipase D activity. *Phys. Chem. Chem. Phys.* 2:4600–4604.

Gil, T., J. H. Ipsen, O. G. Mouritsen, M. C. Sabra, M. M. Sperotto, and M. J. Zuckermann. 1998. Theoretical analyst of protein organization in lipid membranes. *Biochim. Biophys. Acta.* 1376:245–266.

Gliss, C., H. Clausen-Schaumann, R. Günther, S. Odenbach, O. Randl, and T. M. Bayerl. 1998. Direct detection of domains in phospholipid bilayers by grazing incidence diffraction of neutrons and atomic force microscopy. *Biophys. J.* 74:2443–2450.

Harroun, T. A., W. T. Heller, T. M. Weiss, L. Yang, and H. W. Huang. 1999a. Experimental evidence for hydrophobic matching and membrane-mediated interactions in lipid bilayers containing gramicidin. *Biophys. J.* 76:937–945.

Harroun, T. A., W. T. Heller, T. M. Weiss, L. Yang, and H. W. Huang. 1999b. Theoretical analysis of hydrophobic matching and membrane-mediated interactions in lipid bilayers containing gramicidin. *Biophys. J.* 76:3176–3185.

Hinderliter, A., P. F. F. Almeida, C. E. Creutz, and R. L. Biltonen. 2001. Domain formation in a fluid mixed lipid bilayer modulated through binding of the C2 protein motif. *Biochemistry.* 40:4181–4191.

Hunt, J. F., P. D. McCrea, G. Zaccai, and D. M. Engelman. 1997. Assessment of the aggregation state of integral membrane proteins in reconstituted phospholipid vesicles using small angle neutron scattering. *J. Mol. Biol.* 273:1004–1019.

Jørgensen, K., A. Klinger, and R. L. Biltonen. 2000. Nonequilibrium lipid domain growth in the gel-fluid two-phase region of a $DC_{16}PC$-$DC_{22}PC$ lipid mixture investigated by Monte Carlo computer simulation, FT-IR, and fluorescence spectroscopy. *J. Phys. Chem. B.* 104:11763–11773.

Jørgensen, K., and O. G. Mouritsen. 1995. Phase separation dynamics and lateral organization of two-component lipid membranes. *Biophys. J.* 95: 942–954.

Jørgensen, K., M. M. Sperotto, O. G. Mouritsen, J. H. Ipsen, and M. J. Zuckermann. 1993. Phase equilibria and local structure in binary lipid bilayers. *Biochim. Biophys. Acta.* 1152:135–145.

Killian, J. A. 1992. Gramicidin and gramicidin-lipid interactions. *Biochim. Biophys. Acta.* 1113:391–425.

Knoll, W., K. Ibel, and E. Sackmann. 1981. Small-angle neutron scattering study of lipid phase diagrams by the contrast variation method. *Biochemistry.* 20:6379–6383.

Knoll, W., G. Schmidt, H. Rötzer, T. Henkel, W. Pfeiffer, E. Sackmann, S. Mittler-Neher, and J. Spinke. 1991. Lateral order in binary lipid alloys and its coupling to membrane functions. *Chem. Phys. Lipids.* 57:363–374.

Knoll, W., G. Schmidt, E. Sackmann, and K. Ibel. 1983. Critical demixing in fluid bilayers of phospholipid mixtures: a neutron diffraction study. *J. Chem. Phys.* 79:3439–3442.

Koeppe II., R. E., and O. S. Andersen. 1996. Engineering the gramicidin channel. *Annu. Rev. Biophys. Biomol. Struct.* 25:231–258.

Kovacs, F., J. Quine, and T. A. Cross. 1996. Validation of the single-stranded channel conformation of gramicidin A by solid-state NMR. *Proc. Natl. Acad. Sci. U. S. A.* 96:7910–7915.

Landwehr, A., and R. Winter. 1994. High-pressure differential thermal analysis of lamellar to lamellar and lamellar to non-lamellar lipid phase transition. *Ber. Bunsenges. Phys. Chem.* 98:214–218.

Langs, D. A., G. D. Smith, C. Courseille, and G. Précigoux. 1991. Monoclinic uncomplexed double-stranded, antiparallel, left-handed $\beta^{5.6}$-structure of gramicidin A: alternate patterns of helical association and deformation. *Proc. Natl. Acad. Sci. U. S. A.* 88:5345–5349.

Leidy, C., W. F. Wolkers, K. Jørgensen, O. G. Mouritsen, and J. H. Crowe. 2001. Lateral organization and domain formation in a two-component lipid membrane system. *Biophys. J.* 80:1819–1828.

Lindner, P., and Th. Zemb, editors. 1991. Neutron, X-Ray and Light Scattering: Introduction to an Investigative Tool for Colloidal and Polymeric Systems. North Holland, Amsterdam.

Lipowsky, R., and E. Sackmann, editors. 1995. Structure and Dynamics of Membranes, Vols. 1A, 1B. Elsevier, Amsterdam.

Mabrey, S., and J. M. Sturtevant. 1976. Investigation of phase transition of lipids and lipid mixtures by high sensitive differential scanning calorimetry. *Proc. Natl. Acad. Sci. U. S. A.* 73:3862–3866.

May, S., and A. Ben-Shaul. 2000. A molecular model for lipid-mediated interaction between proteins in membranes. Phys. *Chem. Chem. Phys.* 2:4494–4502.

Morrow, M. R., R. Srinivasan, and N. Grandal. 1991. The phase diagram of dimyristoyl phosphatidylcholine and chain-perdeuterated distearoyl phosphatidylcholine: a deuterium NMR spectral difference study. *Chem. Phys. Lipids.* 58:63–72.

Naik, V. M., and S. Krimm. 1986a. Vibrational analysis of the structure of gramicidin A: I. Normal mode analysis. *Biophys. J.* 49:1131–1145.

Naik, V. M., and S. Krimm. 1986b. Vibrational analysis of the structure of gramicidin A: II. Vibrational spectra. *Biophys. J.* 49:1147–1154.

Nielsen, L. K., A. Vishnyakov, K. Jørgensen, T. Bjørnholm, and O. G. Mouritsen. 2000. Nanometre-scale structure of fluid lipid membranes. *J. Phys. Condens. Matter.* 12:A309–A314.

Parasassi, T., E. Gratton, W. Yu, P. Wilson, and M. Levi. 1997. Two-photon fluorescence microscopy of LAURDAN generalized polarization domains in model and natural membranes. *Biophys. J.* 72:2413–2429.

Pascal, S. M., and T. A. Cross. 1993. High-resolution structure and dynamic implications for a double-helical gramicidin A conformer. *J. Biomol. N.M.R.* 3:495–513.

Pfeifer, P., and M. Obert. 1989. The Fractal Approach to Heterogeneous Chemistry: Surface, Colloids, Polymers. D. Avnir, editor. John Wiley and Sons, Chichester. 11–43.

Quist, P.-O. 1998. ^{13}C solid-state NMR of gramicidin A in a lipid membrane. *Biophys. J.* 75:2478–2488.

Sankaram, M. B., D. Marsh, L. M. Gierasch, and T. E. Thompson. 1994. Reorganization of lipid domain structure in membranes by a transmembrane peptide: an ESR spin label study on the effect of the *Escherichia coli* outer membrane protein A signal peptide on the fluid lipid domain connectivity in binary mixtures of dimyristoyl phosphatidylcholine and distearoyl phosphatidylcholine. *Biophys. J.* 66:1959–1968.

Sankaram, M. B., and T. E. Thompson. 1992. Deuterium magnetic resonance study of phase equilibria and membrane thickness in binary phospholipid mixed bilayers. *Biochemistry*. 31:8258–8268.

Sarges, R., and B. Witkop. 1965. The structure of valine and isoleucine-gramicidin A. *J. Am. Chem. Soc.* 87:2011–2020.

Schram, V., and T. E. Thompson. 1997. Influence of the intrinsic membrane protein bacteriorhodopsin on gel-phase domain topology in two-component phase-separated bilayers. *Biophys. J.* 72:2217–2225.

So, P. T. C., T. French, W. M. Yu, K. M. Berland, C. Y. Dong, and E. Gratton. 1995. Time-resolved fluorescence microscopy using two-photon excitation. *Bioimaging.* 3:49–63.

So, P. T. C., T. French, W. M. Yu, K. M. Berland, C. Y. Dong, and E. Gratton. 1996. Two-Photon Fluorescence Microscopy: Time-Resolved and Intensity Imaging in Fluorescence Imaging Spectroscopy and Microscopy, Chemical Analysis Series, Vol. 137. X. F. Wang and B. Herman, editors. John Wiley and Sons, New York. 353–374.

Sugár, I. P., T. E. Thompson, and R. L. Biltonen. 1999. Monte Carlo simulation of two-component bilayers: DMPC/DSPC mixtures. *Biophys. J.* 76:2099–2110.

Sychev, S. V., L. I. Barsukov, and V. T. Ivanov. 1993. The double π, π 5.6 helix of gramicidin A predominates in unsaturated lipid membranes. *Eur. Biophys. J.* 22:279–288.

Urry, D. U. 1971. The gramicidin A transmembrane channel: a proposed $\pi_{(L, D)}$ helix. *Proc. Natl. Acad. Sci. U. S. A.* 68:672–676.

Veatch, W. R., E. T. Fossel, and E. R. Blout. 1974. The conformation of gramicidin A. *Biochemistry.* 13:5249–5256.

Wallace, B. A. 1986. Structure of gramicidin A. *Biophys. J.* 49:295–306.

Wallace, B. A. 1990. Gramicidin channels and pores. *Annu. Rev. Biophys. Chem.* 19:127–157.

Wallace, B. A. 1998. Recent advantages in the high-resolution structures of bacterial channels: gramicidin A. *J. Struct. Biol.* 121:123–141.

Winter, R., A. Gabke, C. Czeslik, and P. Pfeifer. 1999. Power-law fluctuations in phase-separated lipid membranes. *Phys. Rev. E.* 60:7354–7359.

Yu, W., P. T. C. So, T. French, and E. Gratton. 1996. Fluorescence generalized polarization of cell membranes: a two-photon scanning microscopy approach. *Biophys. J.* 70:626–636.

Zein, M., and R. Winter. 2000. Effect of temperature, pressure and lipid acyl chain length on the structure and phase behaviour of phospholipid-gramicidin bilayers. *Phys. Chem. Chem. Phys.* 2:4545–4551.